ABSTRACT

Title of Thesis: MAGNETIC ANISOTROPY OF $Fe_{1-x}Ga_x$ ALLOYS

Sadia Rafique, Master of Science, 2003.

Thesis directed by: Professor Manfred Wuttig
Materials Science and Engineering Department
Adjunct Professor James R. Cullen
Materials Science and Engineering Department

Cubic magnetocrystalline anisotropy constants, K_1 and K_2, for $Fe_{1-x}Ga_x$ alloys were measured using magnetization curves with x = 0.05, 0.125, 0.14, 0.18 and 0.20. Thin circular {110} disks with all <100>, <110> and <111> in the plane of the disk were used to measure K_1 and K_2. K_1 was also measured with {100} circular disks. K_1 for 5 at% Ga content has been found to be larger than that of pure Fe. K_1 and K_2 both drops gradually till 18 % Ga substitution. Then there is a sharp drop in the magnitude of both the constants. <110> and <111> directions were magnetically equivalent for all the compositions considered for this study resulting in K_2 to be equal to $-9K_1/4$. A calculation of anisotropy energy density verifies this result. Magnitude of K_1 measured from both {110} and {100} disks were reasonably consistent.

MAGNETIC ANISOTROPY OF $Fe_{1-x}Ga_x$ ALLOYS

by

Sadia Rafique

Thesis submitted to the Faculty of the Graduate School of the
University of Maryland, College Park in partial fulfillment
of the requirements for the degree of
Master of Science
2003

Advisory Committee:

Dr. Lourdes Salamanca-Riba, Chair
Dr. Ichiro Takeuchi
Dr. James R. Cullen

DEDICATION

To my parents and husband

ACKNOWLEDGEMENT

I would like to acknowledge the invaluable advice and mentoring of my advisors Dr. Manfred Wuttig and Dr. James R. Cullen. I could not have come to this point without their encouragement and guidance.

Many thanks to Dr. Jun Cui for his suggestions and advice and also to other fellow group members: Liyang Dai, Peng Zhao, and Nobuko Koda for their support, and suggestions. I acknowledge the assistance of Ladan Mohaddes-Ardabili, Haimei Zheng and Junlin Wang for helping me through the experimental procedures required for this study.

Finally I would like to thank my husband and my parents for their support and encouragement.

TABLE OF CONTENTS

LIST OF TABLES:

LIST OF FIGURES

Chapter 1

Introduction

1.1 Motivation

Fascinating magnetoelastic and elastic properties of $Fe_{1-x}Ga_x$ alloys have generated considerable interest in such alloys in very recent years. Magnetostriction of FeGa alloys has been found to be so far the largest among all Fe alloys. And these alloys become elastically very soft in certain composition range. Both magnetostrictive and elastic properties are highly dependent on thermal history and composition and both of them follow the same trend as FeAl. Cubic anisotropy constant K_1 of FeAl has been reported to decrease with increasing Al content, goes to zero at some composition and then changes sign [1]. To our knowledge, there has been no work reported on the magnetic anisotropy of FeGa alloys. If anisotropy also follows similar behavior as FeAl, then FeGa alloys become a very interesting category of alloys which are magnetically as well as elastically soft and have very large magnetostriction. This has been the motivation to investigate the magnetic anisotropy of FeGa alloys.

1.2 Work done on FeGa

The magnetostriction of body-centered cubic (bcc) Fe is known for its near compensating constants (λ_{100} = 20 ppm, λ_{111} = -16 ppm) and anomalous temperature dependence. λ_{100} attains a minimum around 400 K and then again rises to a maximum just before the Curie temperature of Fe [2].

In search of a material, which has better magnetic properties than pure Fe in terms of magnetostriction, manetocrystalline anisotropy etc. there have been significant efforts to alloy Fe with various non-magnetic, both transition and non-transition metal elements. These elements include Ti, Co, Ge, Si, Cr, Mo, Al, V etc. Replacement of small amounts of Fe atoms by all of the mentioned elements has impacts on anisotropy and magnetostriction of pure Fe in various degrees [3]. But obtaining an alloy with optimum magnetic as well as elastic properties remained difficult.

Though there has been some work done on magnetic and physical properties of FeGa system and various FeGa alloys in 1960s and early 1970s, it has been only a few years since FeGa alloys have been investigated comprehensively after learning about the intriguing magnetostrictive properties of these alloys.

Figure 1 is the phase diagram of FeGa system.

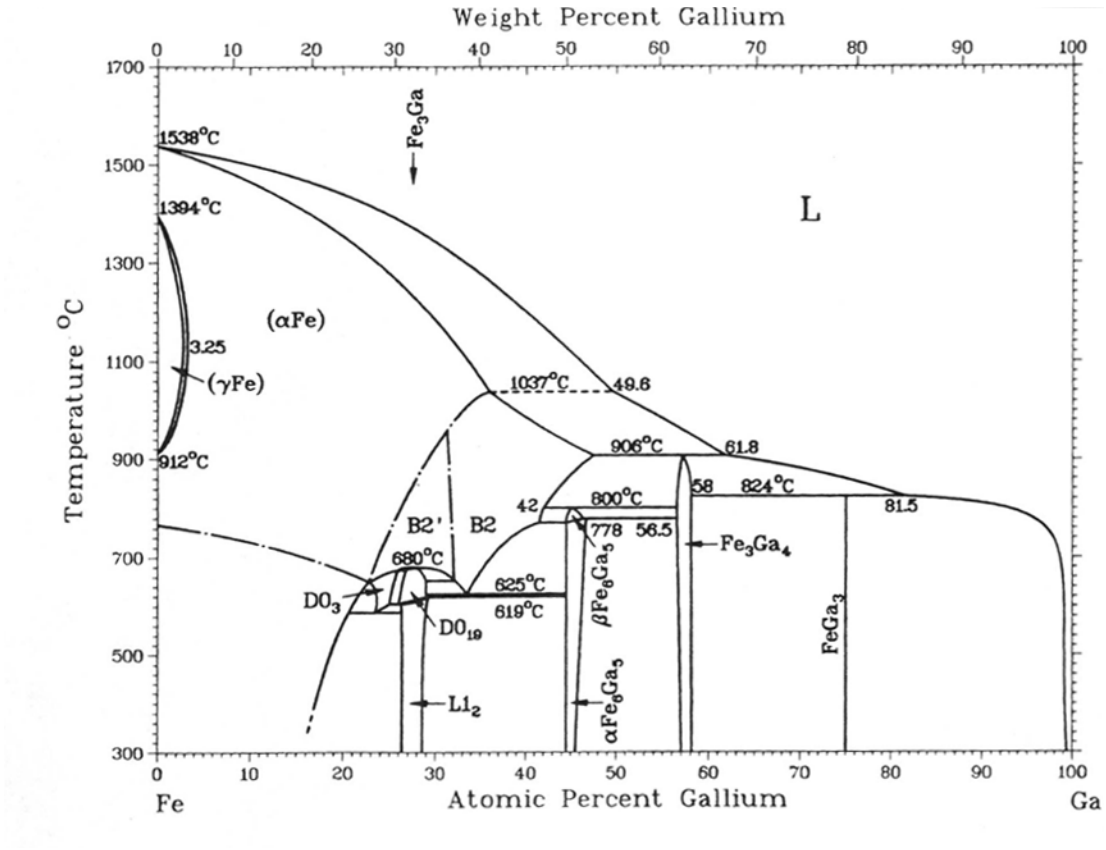

Figure 1: Phase diagram of FeGa alloy system [4]

Ga has large solubility range in Fe. Disordered bcc structure is retained til some point. Both bcc and fcc ordered structures result depending on the thermal treatment. The quenched specimens considered for this report with compositions 5% to 20% Ga should have predominantly bcc structure.

Kawamiya et al. did detail work on physical and magnetic properties of FeGa alloys [5]. They were able to obtain bcc disordered state (α) with 20% Ga by quenching, bcc ordered phase (α", DO_3) with 20% Ga by annealing at 380°C for five hours and fcc ordered phase (β) with 25-30% Ga by annealing for a long time. bcc ordered alloys with composition 23-30% Ga were obtained by quenching but for these alloys neither the disordered nor the ordered phase could be made stable by any quenching method. Figure

2, 3 and 4 show comparison of properties in different final phases of the alloy and their dependence on the composition.

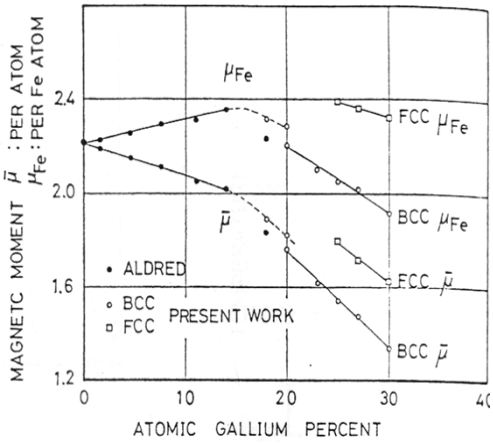

Figure 2: The atomic moment and moment per Fe atom μ_{Fe} as a function of Ga concentration for bcc and fcc FeGa alloys [5]

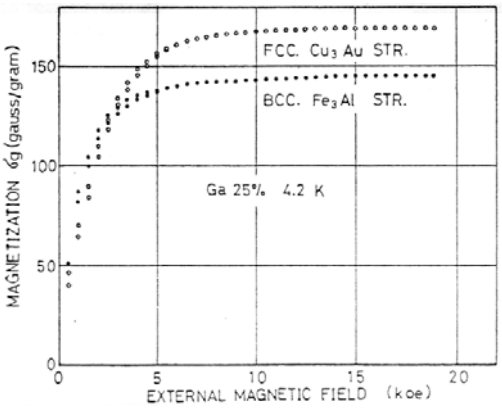

Figure 3: Magnetization as a function of external magnetic field for bcc and fcc Fe_3Ga at 4.2 K [5].

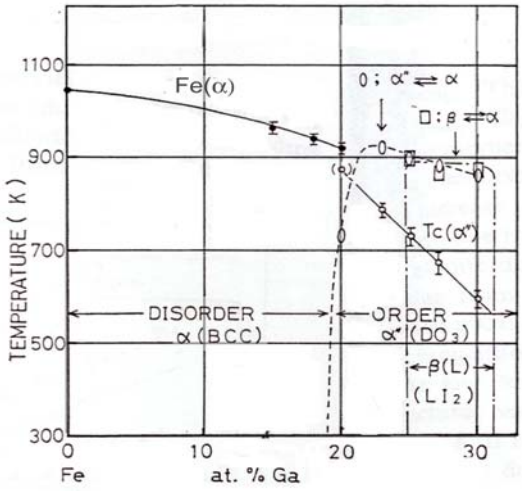

Figure 4: Magnetic phase diagram of FeGa alloy system: the dot-dash line indicates the equilibrium fcc phase and broken line is for quenched bcc phase [5].

Table 1: Data on the magnetic and physical properties of the bcc and the fcc FeGa

Ga %	σ_s (0 K) (emu/g)	$\bar{\mu}$ (μ_B/atom)	μ_{Fe} (μ_B/atom)	D (meVA^2)	T_c (K)	atomic volume (A^3)	lattice const. (A)
(bcc)							
18α	181.0	1.89	2.31	154	940	12.19	2.900_0
20α	174.0	1.82	2.28	150	920	12.26	2.905_0
20α''	167.5	1.76	2.20	137	875*	12.19	2.900_0
23α''	154.1	1.62	2.10	112	790	12.22	2.902_4
25α''	145.0	1.54	2.05	98	730	12.24	2.903_5
27α''	138.2	1.48	2.02	92	675	12.26	2.905_0
30α''	124.7	1.34	1.92	86	595	12.32	2.910_0
(fcc)							
25	169.2	1.80	2.39	191	1040*	12.44	3.678_3
27	162.1	1.72	2.36	179	1015*	12.48	3.681_8
30	151.3	1.62	2.32	169	975*	12.54	3.687_1

FeGa system does not follow the simple dilution in which moment per Fe atom remains constant in spite of alloying. The magnetic moment per Fe atom in FeGa alloys increases with increasing Ga concentration up to 15% then decreases with further increase in Ga concentration.

Of all the substitution alloys, since 1960s FeAl alloys were studied widely after it was found that FeAl alloys having more than 19 at% Al form ordered phases[6]. R.C. Hall has shown that anisotropy constant K_1 for both ordered and disordered FeAl alloys reduces sharply with increasing Al content and goes through zero [1]. The composition of zero anisotropy alloys varies between 22-27 at% Al depending on the degree of ordering which in turn depends on the history of thermal treatment. R.C. Hall also showed that λ_{100} for FeAl reaches the range 80-100 ppm depending on the ordering at around 19 at% Al and then decreases for ordered as well as disordered alloys. In that composition range

increase in λ_{111} is weak and monotonic. Leamy et al [6] has shown that for disordered alloys addition of aluminum to iron decreases $[(C_{11}-C_{12})/2]$ by nearly half of that of Fe

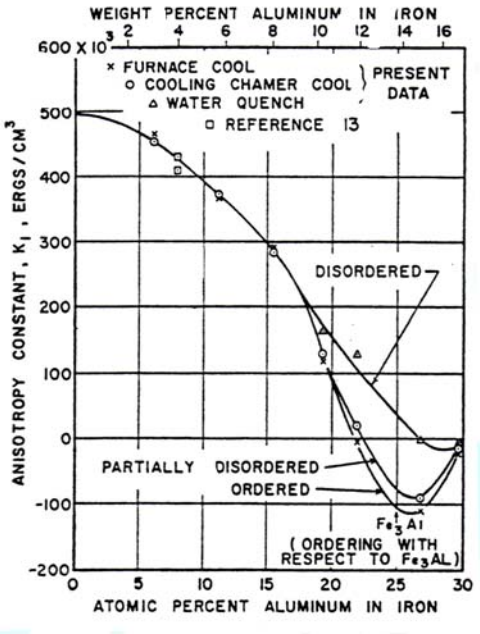

Figure 5: Anisotropy constant K_1 as a function of Al concentration for FeAl alloys [3].

values at 20% Al and increases C_{44}. But C_{44} is a much weaker function Al content than $[(C_{11}-C_{12})/2]$.

Ga and Al both belong to the same group in the periodic table and they share similar electronic configuration. For both elements the outermost electron shell is p shell with one electron. Therefore some similarities in the properties of both the alloys were anticipated. But it has been observed that when Ga is substituted for Fe in the bcc structure, an unprecedented ten-fold increase in the λ_{100} magnetostriction constant occurs (twice the increase in comparable FeAl alloys) [7]. In addition to that, the anomalous dip in the λ_{100} magnetostriction for Fe near room temperature is absent. Instead normal

monotonous decreases in the magnitudes of both λ_{100} and λ_{111} are found. Figure 6 shows the results of the magnetostrictive measurements of FeGa alloys and also shows comparison with FeAl alloys.

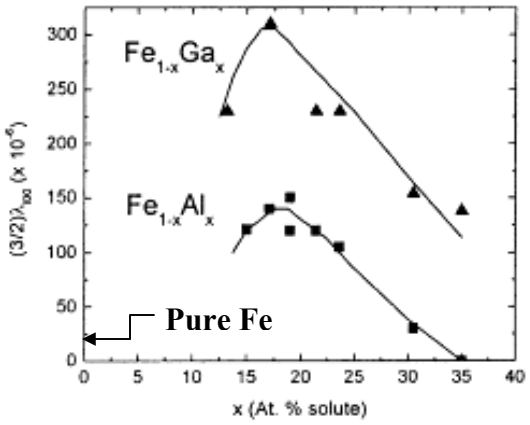

Figure 6: Room temperature saturation magnetostriction for $Fe_{1-x}Ga_x$ and $Fe_{1-x}Al_x$ alloys [8].

It is evident from above results that magnitudes of the saturation magnetostrictions are almost 10 times larger than pure Fe (≈ 20 ppm) and almost twice that of FeAl.

There is a surprising similarity between the concentration dependence of the magnetostriction for both $Fe_{1-x}Ga_x$ and $Fe_{1-x}Al_x$ alloys. In both the cases λ_{100} increases approximately as x^2 until $x \approx 0.18$ (though the degree of increase varies) and then decreases for larger x. One suggestion for the reason of this type of behavior was the presence of cluster of solute atoms (Al or Ga), which act as magnetic and magnetoelastic defects in the alloy [8]. A simple thermodynamic model predicts that at small concentrations, the saturation strain should increase as the number of Al-Al or Ga-Ga pairs i.e. as x^2. For larger concentrations the isolated pairs are gradually replaced by

larger clusters that again respond to magnetization rotation. Many of the pairs are now part of these larger entities, so that the magnetostriction no longer increases as x^2, instead it tends to level off with increasing x. For larger x it is impossible to form the disordered bcc structure, as the alloys are partially of fully DO_3 or B_2 structured. As there are no or very few clusters in the alloy to act as magnetoelastic centers the magnetostriction follows the characteristics of ordered alloy. On the other hand the increase of λ_{111} with x is almost negligible compared to λ_{100} for both the alloys [7]. So the assumption is that there can be no nearest neighbor pairs in <111> direction, because of the size differentials between Ga or Al atoms and Fe atoms. As a result there can be no defect driven contribution to λ_{111}.

After learning about the large magnetostriction of 20 at% FeGa, it was found that this behavior is dependent on the thermal history of the alloy i.e. whether the sample has been quenched or furnace cooled from molten state [9]. This is also true for anisotropy constants of FeAl alloys [3], as has been mentioned earlier in this report. For FeGa alloys, between 19 to 21.4 at% composition the magnetostriction is almost 25% higher for samples that are quenched from 800^{o}C than samples that are furnace cooled at 10^o/min [9]. Figure 7 illustrates the comparison of the magnetostriction between quenched and slow cooled samples. It is evident that for the alloys of the form $Fe_{1-x}Ga_x$, the magnetostriction is independent of thermal treatment till x = 0.17. The peak of the magnetostriction rises 26% and 23% for quenched samples for x = 0.19 and 0.214 respectively. Very recently it has been shown that λ_{100} for $Fe_{1-x}Ga_x$ has a second minimum (Figure 7) again for larger x (≈27% Ga) and this second peak is possibly due to the elastic softening near that composition [10].

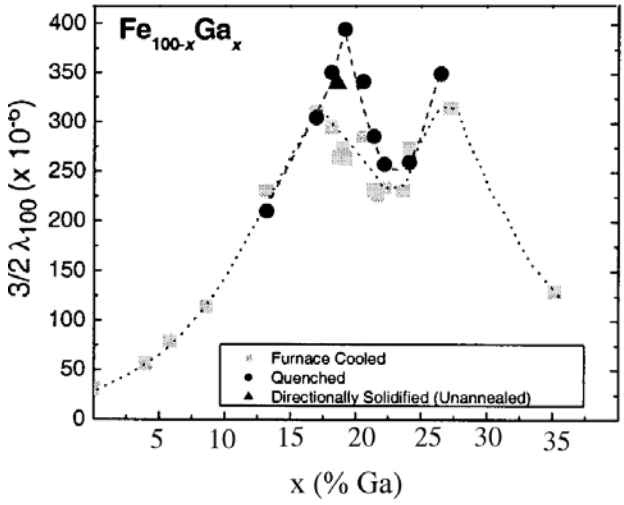

Figure 7: Saturation magnetostriction of $Fe_{1-x}Ga_x$ as a function of Ga concentration [10].

The softening of the shear elastic constant $[(C_{11}-C_{12})/2]$ of the quenched samples of $Fe_{1-x}Ga_x$, investigated by Wuttig et al., helped to explain the magnetostrictive behavior of this alloy [11]. It is reported that while the rhombohedral shear elastic constant C_{44} is independent of Ga composition, the tetragonal shear elastic constant $[(C_{11}-C_{12})/2]$ decreases linearly with increasing Ga content and extrapolates to zero around 26 at% Ga. Figure 8 gives comparison with FeAl data for the same constants. This phenomenon has been attributed to short range atomic order as x increases. The boundaries separating the ordered and disordered regions will produce, under stress, internal deformations which couple to external strain and thereby soften the modulus. Figure 7 shows that the second peak in magnetostriction occurs near that composition.

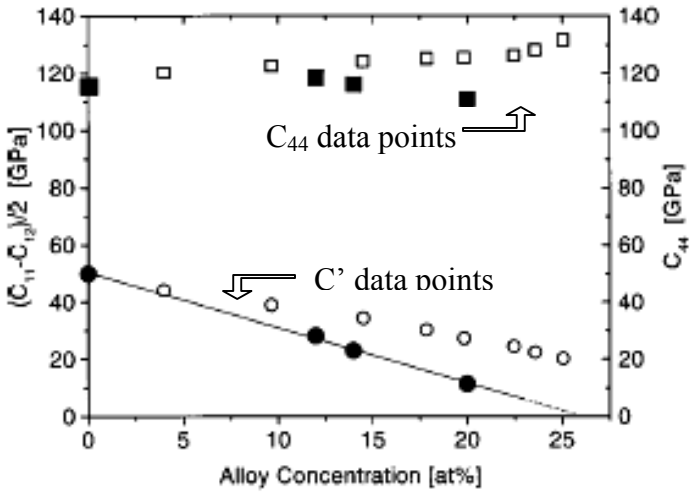

Figure 8: Elastic constants of $Fe_{1-x}Ga_x$ and $Fe_{1-x}Al_x$ alloys as a function of solute concentration. Open symbols represent $Fe_{1-x}Al_x$ alloys and closed symbols represent $Fe_{1-x}Ga_x$ alloys [11].

The experimental evidence of hypothesized short range ordering has been provided by X-ray diffraction pattern [12]. XRD spectra also provided the evidence of structural difference between slow-cooled and quenched conditions which give rise to different values of saturation magnetostriction for the same composition [12]. Figure 9 and Figure 10 are XRD scan of (100) and (111) oriented single crystals for slow cooled and quenched conditions of 19 at% Ga composition.

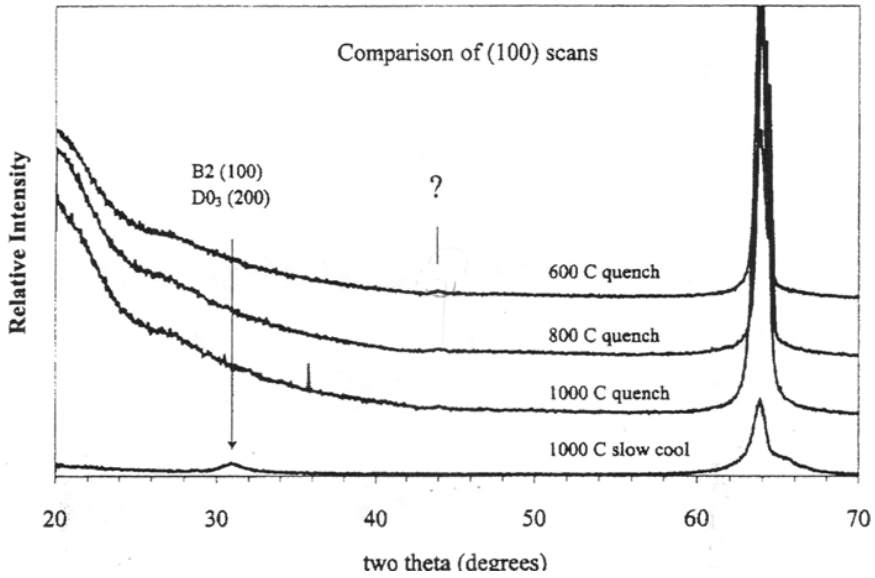

Figure 9: X-ray diffraction scans of a (100) oriented single crystal of $Fe_{1-x}Ga_x$ alloy with x=0.19 for quenched and slow cooled condition [12].

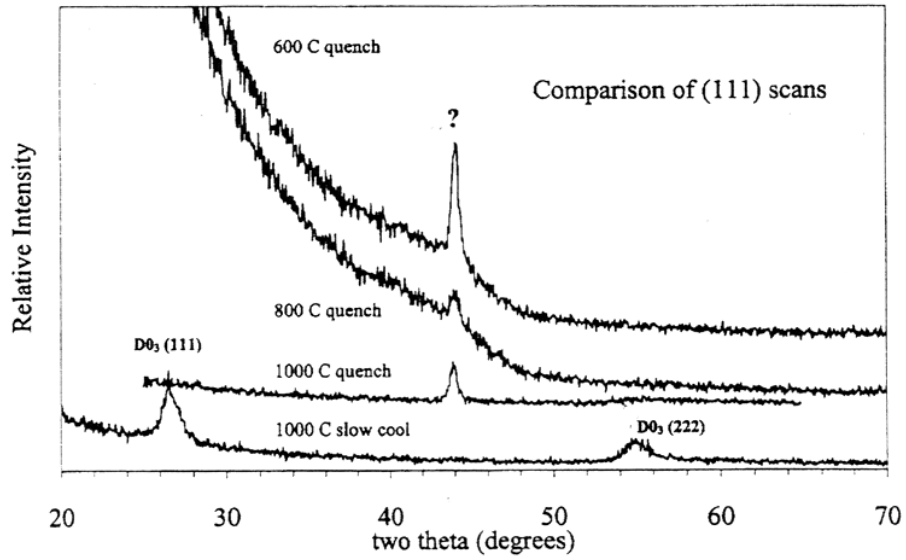

Figure 10: X-ray diffraction scans of a (111) oriented single crystal of $Fe_{1-x}Ga_x$ alloy with x=0.19 for quenched and slow cooled condition [12].

The X-ray data confirm that slow cooling leads to the development of long range ordering of Ga atoms into DO_3 structures. According to the phase diagram an alloy of $Fe_{1-x}Ga_x$ with x=0.19 is in the disordered bcc phase at temperatures above 570^oC. On slow cooling to room temperature, the alloy enters into a two-phase region of bcc+$L1_2$ (ordered fcc Fe_3Ga). However the kinetics of the precipitation of $L1_2$ is extremely slow and the alloy tends to order into the metastable DO_3 arrangement. In contrast, when the alloy is quenched from the disordered state, the long-range DO_3 ordering is suppressed, and all the superlattice reflections associated with the DO_3 long-range order are extinct.

The unexpected development of peak at ≈44^o in both (100) and (111) orientations in the quenched condition led to the alternative schemes or arrangements of Ga atoms in unit cell as the peaks were not consistent with either the disordered bcc or the long range ordered DO_3 and $L1_2$ structures. In consistent with the proposition of Ga pairing along <100> a modified DO_3 or a FCT unit cell was assumed and the X-ray diffraction pattern was calculated. It was found that this sort of tetragonal distortion of the matrix could explain the experimental diffraction pattern. But the low intensity of the peak is indicative of the fact that only a small volume fraction of the bcc matrix undergoes tetragonal transformation on quenching.

In order to explain the extra-ordinary magnetostriction of these alloys from electronic and atomic origin similar kind of tetragonal atomic arrangement (named as B_2-like, Figure 11), taking into account of the Ga pairs along <100> directions, was assumed [13]. The magnetostriction value calculated from this structure was comparable to experimental values of λ_{100} for B_2-like structures but obtained opposite signs for DO_3 or $L1_2$ structures for 25 at% composition.

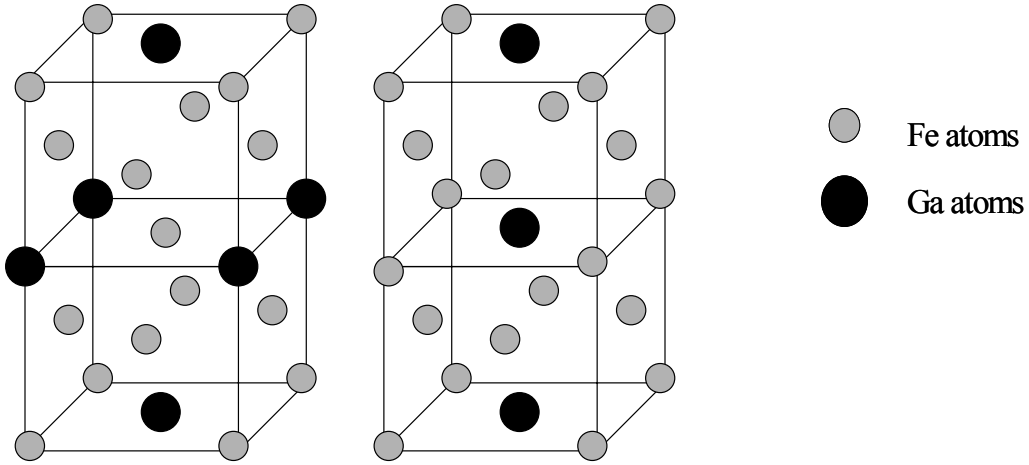

Figure 11: B_2-like structure proposed by Wu [13]

Chapter 2

Theoretical Background

2.1 Definition of Magnetocrystalline Anisotropy

The dependence of the internal energy of a magnetic material on the direction of spontaneous magnetization is called the magnetic anisotropy. The magnetization tends to lie in certain preferred directions giving rise to an anisotropy in magnetization in the crystal. The anisotropy can be intrinsic, related to atomic scale interactions, which define easy directions in the crystal (magnetocrystalline anisotropy), or it can be related to the energy of the sample in its own demagnetizing field (shape anisotropy). In this report we discuss only magnetocrystalline anisotropy energy.

2.1 Origin of Anisotropy

There are several explanations of anisotropy in terms of atomic and crystal structure. The quantum forces of exchange that are responsible for the molecular field are isotropic in character and do not account for the variation of properties with direction. One of the first proposals regarding the origin of anisotropy considered the magnetic interaction between magnets of various kinds, located at the lattice points of the crystal [14]. The magnetic action of a cubic lattice of dipole moments, always aligned parallel to each other, is purely isotropic. On the contrary, if bar-shaped magnets are located at the points of a body-centered lattice such as iron, they will have stable positions when they are parallel to cube diagonal, [111]. If the magnets are formed by current loops or are small, flat, disk-shaped permanent magnets magnetized perpendicular to the surface; they

are stable when parallel to [100]. Agreement with experiments is thus obtained if the atomic magnets in iron are assumed to be disk-shaped. Similarly it has been shown that one can explain qualitatively the direction of easy magnetization in nickel, [111], if one assumes that here the atomic magnets are bar-shaped (elongated in the direction of magnetization).

More realistic atomic model showed that interaction of a purely magnetic nature is quantitatively deficient by a factor of approximately 1000, which led to the invocation of spin-orbit coupling. In the solid lattice the electron orbits are restricted by the electrostatic fields of neighboring atoms so that they cannot be freely oriented by a magnetic field. There is also strong electrostatic interaction between the spin and orbital motion of a single electron. Consequently, when the external magnetic field orients the spin of one electron, it reacts on its own orbit, which reacts on the orbits of the neighboring atoms, which, in turn, influence the spins in these orbits. The directional character of the orbits is thus communicated to the spins.

The most tangible and complete calculation of the spin-orbit coupling was given by Van Vleck [14]. His models were able to explain the anisotropy constants with right order of magnitude, general dependence of the anisotropy constants with temperature etc. Further modeling by electron bands resulted in agreement with the general experimental value of anisotropy constant, signs of the constants for iron and nickel and change of sign of the constant of iron-nickel alloy with composition etc [14].

2.3 Measuring Magnetic Anisotropy

Magnetocrystalline anisotropy energy density, E_k , of a cubic material is expressed in terms of anisotropy constants and is a function of direction cosine of the magnetization vector with the crystal axes. For a cubic crystal the energy is expressed as

$$E_k = K_0 + K_1 (\alpha_1^2\alpha_2^2 + \alpha_2^2\alpha_3^2 + \alpha_3^2\alpha_1^2) + K_2\alpha_1^2\alpha_2^2\alpha_3^2 + \ldots \quad (1)$$

α_1, α_2 and α_3 are the direction cosines (angle that magnetization vector makes with the crystalline axes) and K_0, K_1 and K_2 are the anisotropy constants. For most practical purposes K_1 and K_2 are the most important anisotropy constants. There are various means of measuring anisotropy. Some of them are discussed below:

2.3.1 Torque curves

One of the most reliable methods of determining anisotropy is by measuring the torque that exists when an anisotropic crystal is placed in a uniform magnetic field. The torque magnetometer is the apparatus, which is commonly used for this purpose. Usually the specimen is suspended by a fine elastic string between the pole pieces of a rotatable electromagnet. When a strong magnetic field is applied to the specimen, the internal magnetization is forced to line up with the field, and the specimen disk itself tends to rotate so as to make an easy direction approach the direction of magnetization. The torque exerted by the specimen can be measured by the angle of twist of the elastic string. If the magnet is rotated, the torque can be measured as a function of crystallographic direction of magnetization. We call this curve a magnetic torque curve, from which we can reproduce the magnetic anisotropy energy.

Calculation: The torque acting on each unit volume of a crystal is equal to the rate of change of energy density with angle:

$$L = -dE/d\theta$$

θ denoting the angle between the direction of magnetization and a crystallographic axis. For magnetization confined to a (001) plane of a cubic crystal, $\alpha_1 = \cos\theta$, $\alpha_2 = \sin\theta$ and $\alpha_3 = 0$. Then the first term of equation (1) becomes

$$E_k = K_1 \cos^2\theta \sin^2\theta = \frac{1}{4} K_1 \sin^2 2\theta$$

From the above relationship of torque and anisotropy energy we get

$$L = -\frac{1}{2} K_1 \sin 4\theta$$

K_1 can then be obtained by fitting the experimental L vs θ curve.

Similarly in the (110) plane where K_1 and K_2 are both involved, the constants can be adjusted by obtaining a best fit to the experimental data. (111) plane can also be used to determine K_2.

2.3.2 Ferromagnetic Resonance

The magnetic anisotropy can also be measured by means of the ferromagnetic resonance. The resonance frequency depends on the external magnetic field, which exerts a torque on the precessing spin system. Since a magnetic anisotropy also causes a torque on a spin system if it points in a direction other than an easy direction, the resonance frequency is expected to be dependent on the magnetic anisotropy.

Calculation: When a ferromagnetic resonance is observed by applying a magnetic field parallel to the easy direction, the resonance frequency should be given by

$$\omega = \nu(H + H_a)$$

where H_a is the anisotropy field and H is the applied magnetic field. This means that the resonance occurs at an external field lower than in the isotropic case by H_a.

For the cubic anisotropy, the direction cosines in polar coordinates are as follows:

$$\alpha_1 = \sin\theta\cos\phi \approx \theta\cos\phi$$

$$\alpha_2 = \sin\theta\sin\phi \approx \theta\sin\phi$$

$$\alpha_3 = \cos\theta \approx 1 - \frac{1}{2}\theta^2$$

for $\theta << \pi$, so that the second term of equation (1) becomes (ignoring higher terms for the moment)

$$E_a = K_1[\theta^4 \sin^2\phi\cos^2\phi + (1 - \frac{1}{2}\theta^2)^2\theta^2] \approx K_1\theta^2$$

Anisotropy field is given by

$$H_a = 2\frac{K_1}{I_s}$$

for <100> directions where I_s is the saturation magnetization. When the magnetization is nearly parallel to the <111> directions, the anisotropy energy can be expressed by

$$E_a = \frac{K_1}{3} - \frac{2K_1}{3}\theta^2$$

and the anisotropy field is

$$H_a = -\frac{4K_1}{3I_s}$$

Therefore, when the field is rotated from <100> to <111>, the shift of the resonance field is changed by the amount

$$\Delta H = \frac{2K_1}{I_s} - \left(-\frac{4K_1}{3I_s} \right) = \frac{10K_1}{3I_s}$$

K_1 can then be estimated from the H vs θ curves in <100> and <111> directions.

2.3.3 Magnetization curves

Magnetic anisotropy can also be estimated from the magnetization curves of the single crystals. This method has been followed for this report. There are various ways single crystal magnetization curves can be used to determine magnetic anisotropy. But the most convenient way is to calculate it from the area enclosed by the magnetization curve and the magnetization axis.

Calculation: The difference in the crystal anisotropy energy density between two different crystal directions can be determined by measuring the difference in energy necessary to magnetize a crystal in these two directions. This comes from the fact that total energy of a magnetic body under external magnetic field is the summation of anisotropy and magnetic potential energies,

$$E_{Total} = E_K + E_I$$

$$= E_K - I.H$$

where I is the magnetization and H is the magnetic field. Minimizing total energy with respect to I gives the following

$$dE_K = HdI$$

$$\text{therefore, } E_K = \int HdI$$

From this we can state that the work needed to magnetize a crystal in a particular direction is

$$A_{hkl} = \int_0^{I_s} HdI$$

which is the area under the magnetization curve for a given direction [hkl] with field of magnitude H and the magnetization axis. When we take the difference in the area in two different directions, other forces like magnetostriction contributing to

$\int$HdI are eliminated. So the difference in A for any two directions is equal to the difference in E_k for these directions.

If [110] and [100] are the two directions along which A is measured then the corresponding direction cosines are (1/√2,1/√2,0) and (1,0,0). Substituting in equation (1) we get:

$$A_{110} - A_{100} = E_{110} - E_{100} = K_1/4$$

similarly

$$A_{111}\text{-}A_{100} = K_1/3 + K_2/27$$

and conversely

$$K_o = A_{100} \qquad (2)$$

$$K_1 = 4\,(A_{110} - A_{100}) \qquad (3)$$

$$K_2 = 27(A_{111}\text{-}A_{100}) - 36(A_{110}\text{-}A_{100}) \qquad (4)$$

K_1 can then be determined by measuring the area between the magnetization curves for the [100] and [110] directions and K_2 by measuring A_{111}-A_{100} using the curve for [111].

In order to determine crystal anisotropy in a tetragonal system by this method, the expression for the anisotropy energy is

$$E_k = K_0 + K_1 \sin^2\phi + K_2 \sin^4\phi + K_3 \cos^2\alpha \cos^2\beta$$

where ϕ is the angle between the magnetization and the tetragonal axis, [001], and α and β are the angles with the other two axes. This leads to

$$E_{001} = K_0$$

$$E_{100} = E_{010} = K_0+K_1+K_2$$

$$E_{110}=K_0+K_1+K_2+K_3/4$$

The K's can be evaluated by use of the relations

$$E_{100}-E_{001}=K_1+K_2$$

$$E_{110}-E_{100}=K_3/4$$

K_1 and K_2 can be determined separately in crystals of this symmetry from the shape of the I vs H curve in a direction of difficult magnetization.

In case of uniaxial anisotropy the anisotropy constant (K_u) is the area under the magnetization curve when the applied field is perpendicular to the easy direction.

For good single crystal specimens with no hysteresis in the magnetization curves this method of determination of anisotropy energy seems to be the most straightforward one.

Chapter 3

Sample preparation and experimental method

3.1 Sample preparation

Quenched single crystal specimens of $Fe_{1-x}Ga_x$ alloy with x = 0.05, 0.125, 0.14, 0.18 and 0.20, grown by Bridgman Technique by Ames Laboratory in Iowa State University, were used for this study. The orientation of the rectangular prism specimens is shown in Figure 12. For magnetization measurement two sets of thin circular disks with <110> normal and <100> normal were cut by EDM (Electrical Discharge Machining). {110} disk had <100>, <110> and <111> directions in the plane of the disk. Similarly {100} disk had two <100> directions perpendicular to each other in the plane of the disk. All these directions were marked in the sample while cutting. Figure 12 illustrates the samples used. The disks were 3.5 to 5mm in diameter and the diameter to thickness ratio was kept ≥ 10:1 to ensure the magnetization in the plane of the disk. Magnetization measurements were performed along <100>, <110> and <111>directions for {110} disks and along <100> and at an angle 45^o with <100> to have the <110> direction for {100} disks. Both the cubic magnetocrystalline anisotropy constants K_1 and K_2 could be obtained from {110} disks. K_1 could also be obtained from {100} disks and two sets of K_1 values were matched in order to ensure consistency.

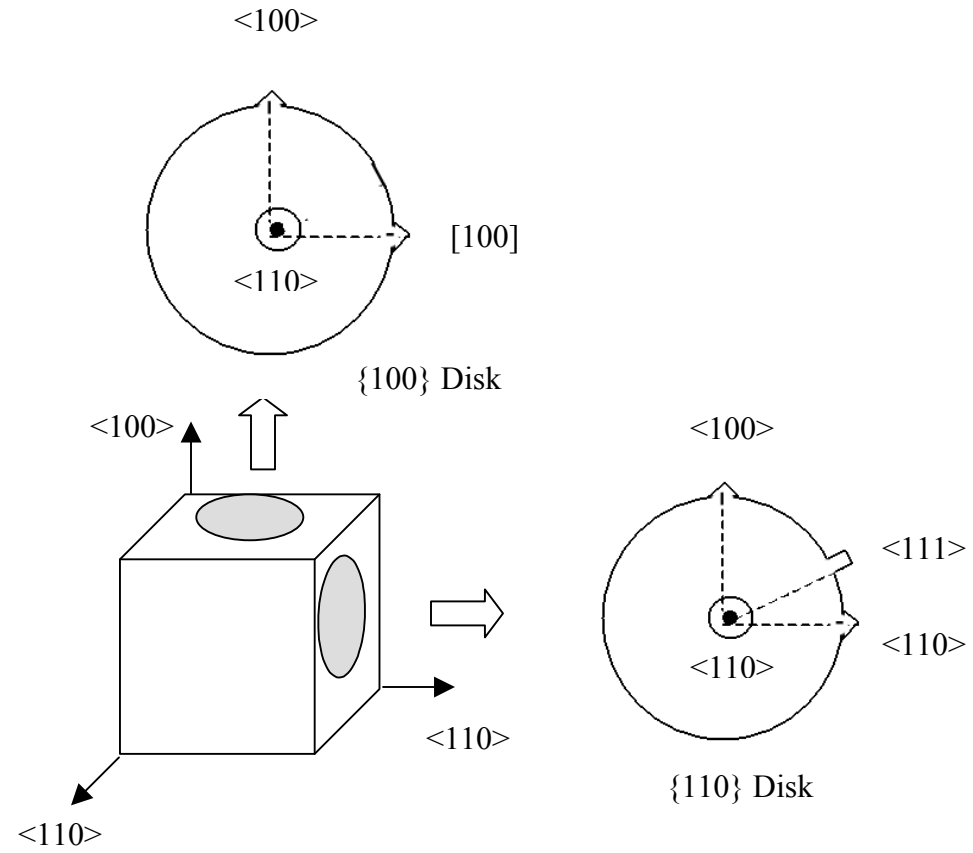

Figure 12: Samples used for the study.

3.2 Experimental Method

Magnetization curves were obtained by a Lakeshore Vibrating Sample Magnetometer (VSM, Model 7300). The operating principle of a VSM is given in the appendix.

The data obtained from VSM was in terms of magnetic field (Oersted) and moment (emu). The moment was converted into the magnetization (emu/cc) value. Magnetization vs field data was plotted in Excel and the area between the magnetization curve and magnetization axis was then measured with the help of Origin 6.0 professional software.

Chapter 4

4.1 Results

Following are the magnetization curves obtained from {110} disk.

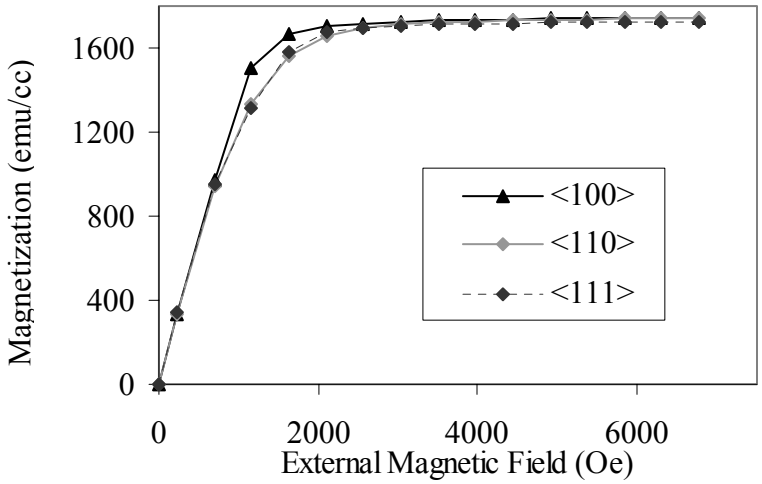

Figure 13: Magnetization curves vs external magnetic field for $Fe_{1-x}Ga_x$ alloy with x = 0.05 obtained from {110} disk.

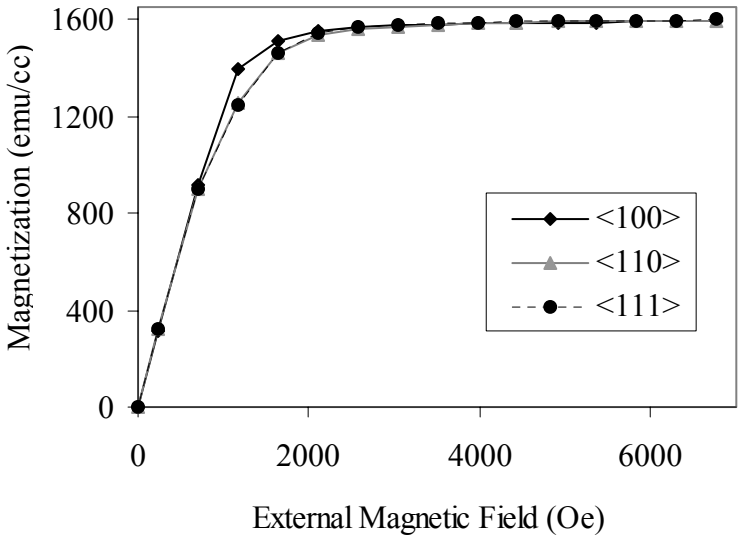

Figure 14: Magnetization curves vs external magnetic field for $Fe_{1-x}Ga_x$ alloy with x = 0.125 obtained from {110} disk.

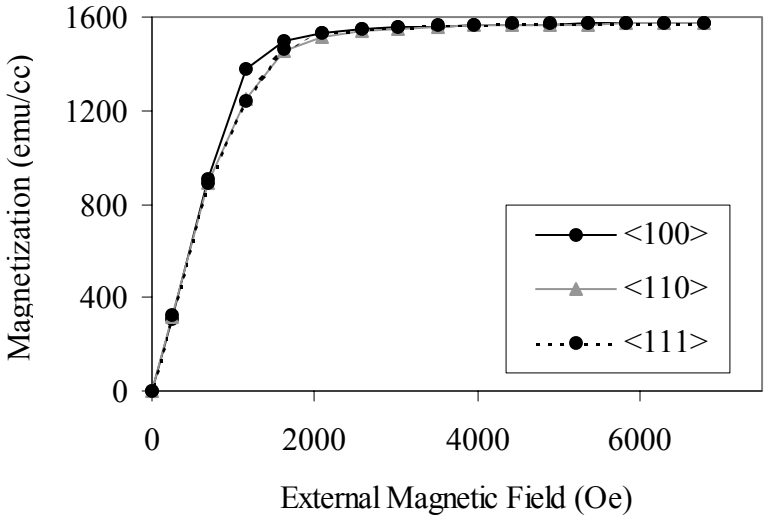

Figure 15: Magnetization curve vs external magnetic field for $Fe_{1-x}Ga_x$ alloy with x = 0.14 obtained from {110} disk.

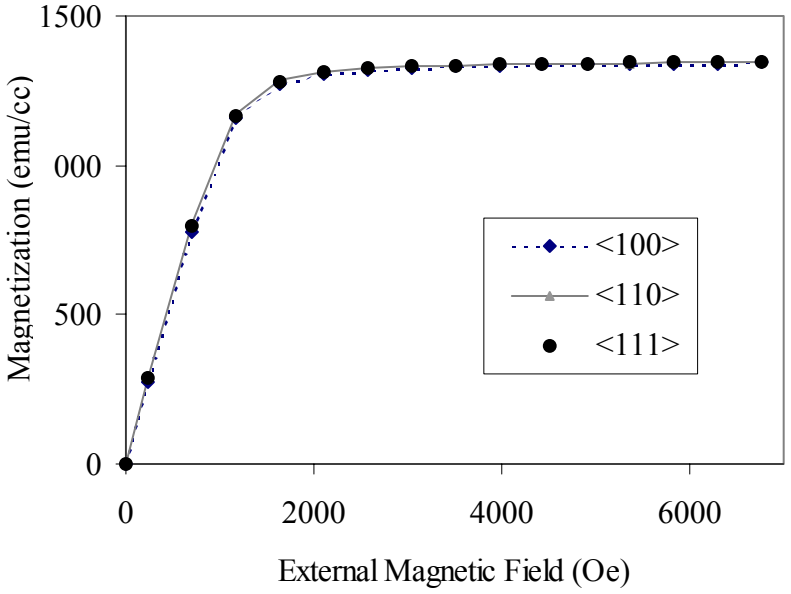

Figure 16: Magnetization curve vs external magnetic field for $Fe_{1-x}Ga_x$ alloy with x = 0.20 obtained from {110} disk.

Following are some typical magnetization curves obtained from {100} disks

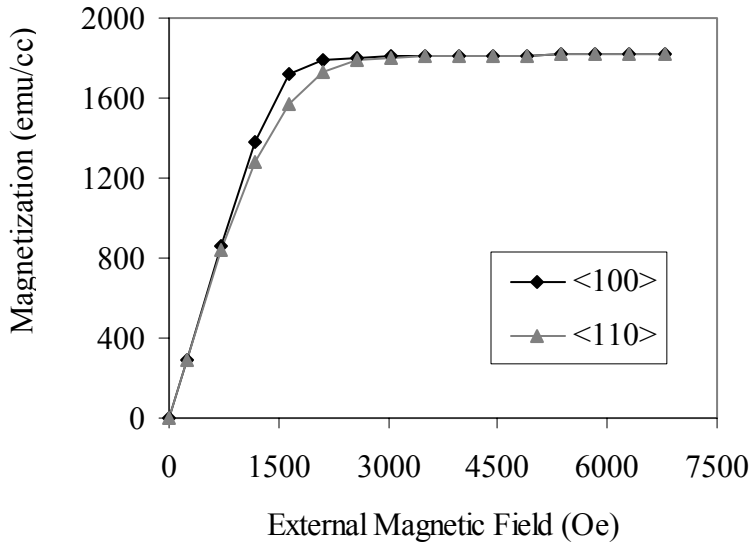

Figure 17: Magnetization curves vs external magnetic field for $Fe_{1-x}Ga_x$ alloy with x = 0.05 obtained from {100} disk.

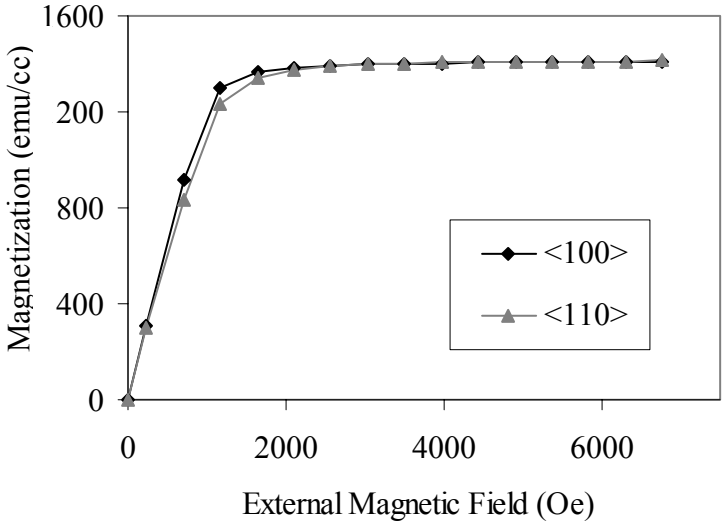

Figure 18: Magnetization curves vs external magnetic field for $Fe_{1-x}Ga_x$ alloy with x = 0.18 obtained from {100} disk.

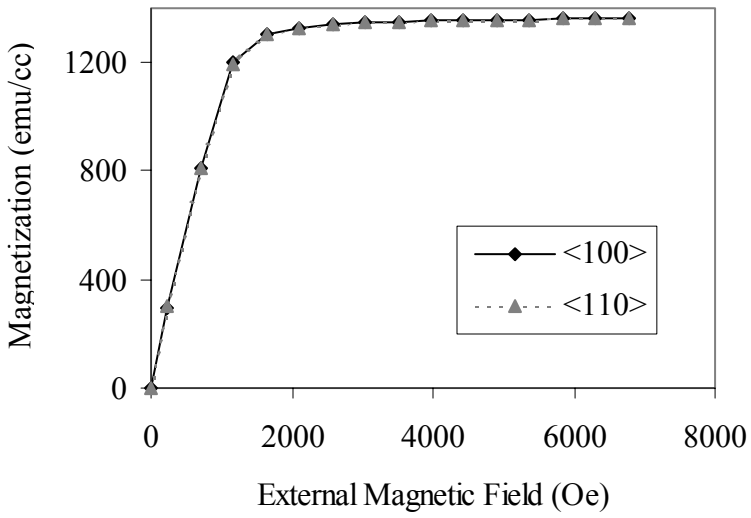

Figure 19: Magnetization curves vs external magnetic field for $Fe_{1-x}Ga_x$ alloy with x = 0.20 obtained from {100} disk.

Following are the key features that are observed from the magnetization curves shown above:

1. <100> is the easy axis for all the compositions (also mentioned by Kawamiya et al.[5]).
2. There is no hysteresis observed for any of the compositions.
3. The samples are quite saturated with the magnitude of the applied field (≈7 kOe)
4. <110> and <111> seems to be equally hard for all the compositions. There is very little area observable (within the used scale) between the magnetization curves in these two hard directions.
5. Though Ga is non-magnetic, Ga initially increases the moment of Fe [5]. It is observable from these experiments also. $Fe_{1-x}Ga_x$ with x = 0.05, the saturation moment (≈ 1745 emu/cc) is very close to that of pure Fe (1745 emu/cc) [15]. But saturation magnetization gradually decreases as Ga substitutes more and more Fe (see Table 2). Also the samples seem to start saturating by weaker magnetic field with increasing Ga composition. Both these observations indicate that the material is becoming softer and the anisotropy is decreasing.
6. Close observation of the figures reveals that when applied field is along a hard direction, magnetization tends to go along easy direction upto a certain point and then breaks away from that and eventually goes to saturation.
7. There is some observable area between the magnetization curves along <100> and <110> (or <111>) directions for 5, 12.5, 14 and 18 at% compositions. This area does not change much till alloy composition is 18 at %. But there is almost no area between the curves when we reach 20% composition. Magnetization curves

in all directions seem to fall on each other for this particular composition (true for both {110} and {100} disks).

It is mentioned earlier that the area between the magnetization curves in different crystallographic direction is a measure of the magnetocrystalline anisotropy for a magnetic material. Because the difference in the area signifies the difference in the energy required to magnetize a material in that particular direction from the direction of spontaneous magnetization. From observation we can say that there is some anisotropy for alloy compositions 5, 12.5, 14 and 18%. This anisotropy decreases gradually as the alloy becomes richer in Ga composition. But the fact that there is almost no area between the magnetization curves for 20% sample indicates that anisotropy is very low, almost none, for that composition. This sudden drop in anisotropy is evident in the values of anisotropy constants K_1 and K_2 which were calculated using equation (3) and (4).

Table 2 lists all the calculated values of the anisotropy constants K_1 and K_2 and Figures 20 & 21 shows the trend of the constants with alloy composition.

Table 2: Calculated values of the anisotropy constants, K_1 and K_2.

Composition	Saturation magnetization	K_1 From {110} Disk	K_1 From {100} Disk	K_2 From {110} Disk	$K_2 = -9K_1/4$
at% Ga in Fe	emu/cc	J/m^3	J/m^3	J/m^3	J/m^3
0	1745*	4.8×10^4*		-3×10^2*	
5	1745	6.56×10^4	6.26×10^4	-1.35×10^5	-1.48×10^5
12.5	1590	4.88×10^4	4.63×10^4	-1.10×10^5	-1.10×10^5
14	1575	4.56×10^4	4.38×10^4	-9.64×10^4	-1.03×10^5
18	1406	NA	3.49×10^4	NA	-7.68×10^4
20	1343	-2×10^3	3.23×10^2	1.43×10^4	4.50×10^3

* Values for pure Fe have been taken from reference [15].

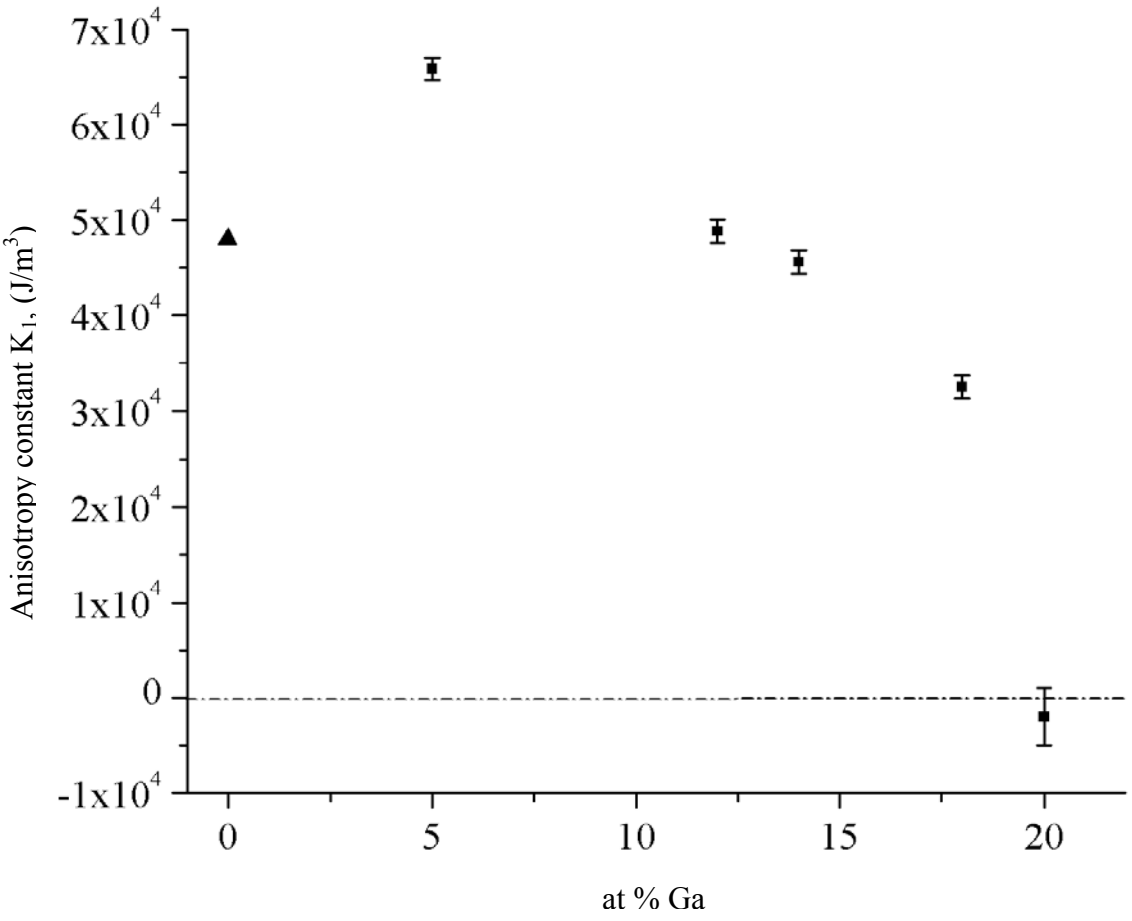

Figure 20: Anisotropy constant K_1 vs x for $Fe_{1-x}Ga_x$ alloys.

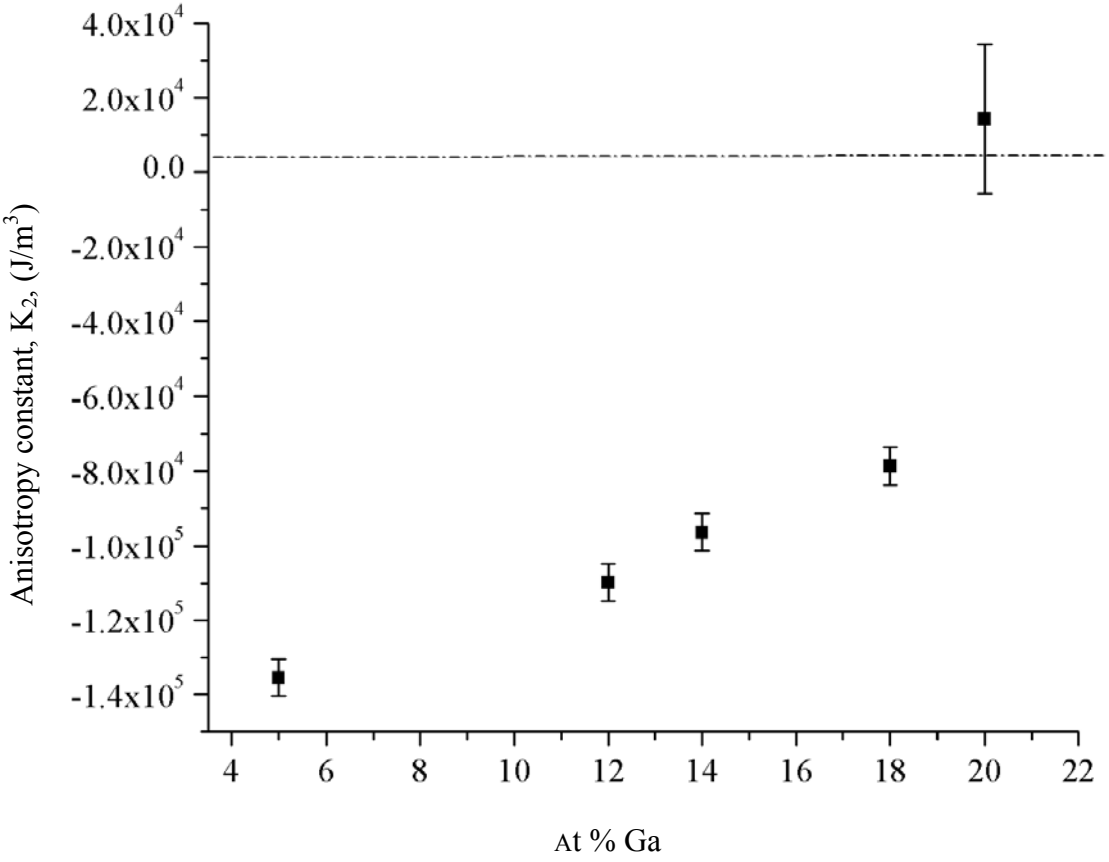

Figure 21: Anisotropy constant K_2 vs x for $Fe_{1-x}Ga_x$ alloys.

It is to be mentioned here that the magnitude of the anisotropy constants for Fe.80Ga.20, which is very small, falls in the error range of the magnetometer used for this study. So it was very difficult to get a consistent value of K_1 and K_2 for that composition. The calculated values fell both in negative and positive range. That is why error bar used in Figure 20 and Figure 21 for 20% sample is larger than the rest of the samples and covers both negative and positive range. Further discussion in this report focuses on the drop of the magnitude of the anisotropy constants at 20% composition and not on the actual magnitude of the constants.

Chapter 5

Discussion

5.1 Analysis of Result

The key features of the results are:

1. The value of the anisotropy constant initially increases with the substitution of non-magnetic Ga to pure Fe. This is in contrast with FeAl (Figure 5) where K_1 begins to drop as soon as Al is substituted in Fe. As has been mentioned earlier in this report that the extraordinary softening of the tetragonal shear constant and the increase in λ_{100} along [100] direction in FeGa and FeAl alloys has so far been attributed to the Ga pairs or Al pairs, basically the solute pairs in <100> directions. The hypothesis is that these solute pairs act as elastic and magnetoelastic defects in the alloy that increases the saturation strain at small concentration. As the concentration of the solute pairs increases it becomes impossible to preserve disordered bcc structures. These solute pairs in <100> directions could be a reason of a preference of spontaneous magnetization towards <100> directions and as a result we see anisotropy constants higher than pure Fe. Although the pairs do not give rise to hysteresis at any compositions, the preference for <100> is apparent at a concentration as low as 5% Ga. As the alloy becomes richer in Ga composition, <100> direction is still preferred but the magnitude of the anisotropy constant decreases gradually as the system approaches to more and more ordered regime.

2. There is a sudden drop in anisotropy at 20% Ga composition for both the constants. At this composition the preference towards any crystalline direction breaks down and all the directions are magnetically equivalent. This drop in anisotropy at 20% composition is not completely unexpected for two reasons. Firstly, the alloy enters into new DO_3 ordered phase at this composition as evident from the phase diagrams (Figure 4 and Figure 5) and the new ordered phase is contributing to lowering of anisotropy.

   The theoretical calculation of anisotropy energy by Wu [13] suggests that DO_3 structure has nearly zero anisotropy for 25%. Assuming that there is not much difference between 20 and 25% composition, this calculation agrees with our results and may explain why K_1 and K_2 are so small around that composition.

   Secondly, magnetic phase diagram shows increasing non-magnetic Ga in the alloy leads to the decrease in the Curie temperature and also shows that the Curie temperature drops more rapidly in the ordered phase. This also leads to decrease in anisotropy.

3. The other key feature of this study is that magnetization along two hard directions, <111> and <110>, is equivalent for all compositions and results in a relationship: K_2 is equal to $-9K_1/4$. Similar phenomenon is present $Ni_{51.3}Mn_{24.0}Ga_{24.7}$ over a range of temperature down to the martensitic start temperature [17].

   In order to understand this behavior, further calculation was performed. First we wanted to see how the magnetization curves look in arbitrary directions

other than the major crystalline directions in the sample. Magnetization data were acquired along the directions shown in Figure 22 and Figure 23 shows the magnetization curves obtained for a 5% sample (5% sample was arbitrarily chosen).

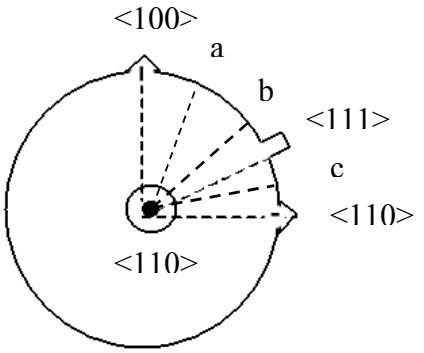

a = direction at 35 degree angle with <100>
b = direction at 45 degree angle with <100>
c = direction at 75 degree angle with <100>

Figure 22: {110} disk with different crystalline directions.

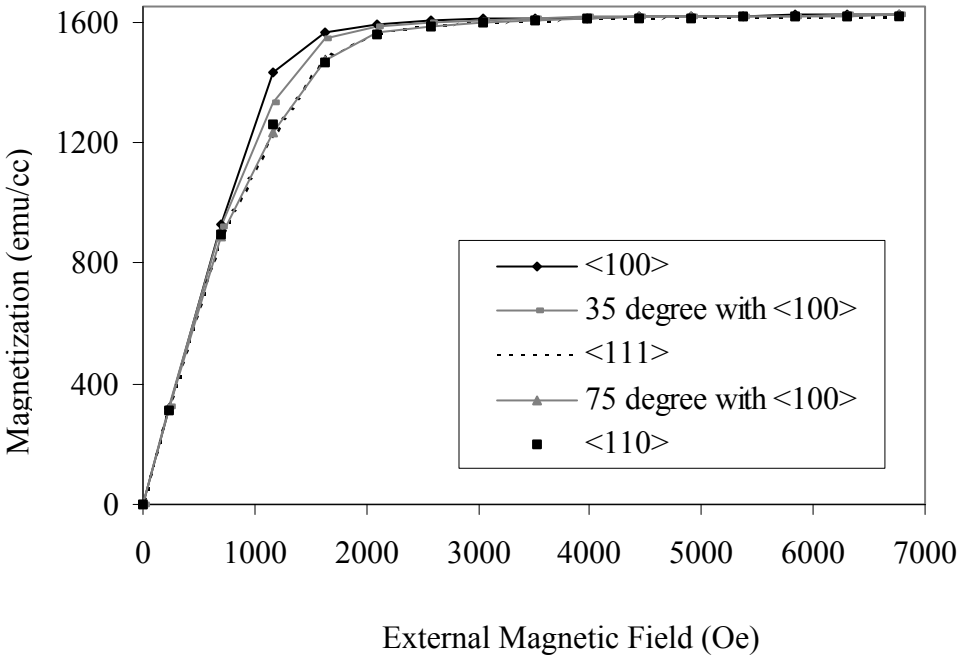

Figure 23: Magnetization curves vs external magnetic field for $Fe_{1-x}Ga_x$ alloy with x = 0.05 for several different directions.

Figure 23 shows that magnetization curve along a direction that lies at 35^o with <100> is at an intermediate position. But there is very little difference between the curves along <111> (54.7^o with <100>), a direction with 75^o with <100> and <110> (90^o with <100>).

The next step was to analyze the rotational model of magnetization, the underlying model of magnetization for this anisotropy analysis, using experimental data and using the relationship between K_1 and K_2 ($K_2 = -9K_1/4$). The idea was to verify the suitability of the model for this alloy system. The analysis is as follows:

Total energy of the crystal under magnetic field is the summation of the anisotropy energy and the magnetic potential energy. We were interested to see how this energy of the crystal varies as a function of angle as the magnetization rotates away from easy direction with applied field along hard direction. Assuming the magnetization is in {110} plane and corresponding direction cosines are:

$$\alpha_1 = \alpha_2 = \sin\theta/\sqrt{2} \text{ and } \alpha_3 = \cos\theta$$

Substituting these into equation (1) and using $K_2 = -9K_1/4$ we get the following relationship anisotropy energy in terms of θ:

$$E_K = 1/4\sin^4\theta + 7/16\sin^2\theta\cos^2\theta$$

To find the potential energy the configuration in Figure 24 was assumed.

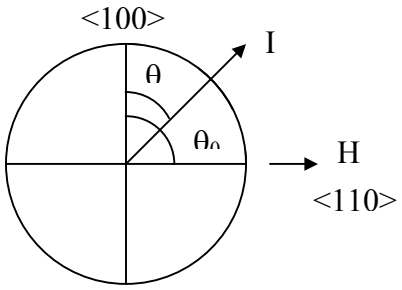

Figure 24: Sample showing the angles of magnetization vector and magnetic field with respect to easy axis of magnetization.

Here applied field H is along hard direction <110>. θ_0 is the angle between the magnetic field and the easy axis and is equal to 90^o for this configuration. Magnetization I makes angle θ with easy axis and the potential energy can now be expressed as

$$E_I = -I_s \frac{H}{K}\cos(\theta - \theta_0)$$

Thus the total energy becomes:

$$E_{Total} = 1/4\sin^4\theta + 7/16\sin^2\theta\cos^2\theta - I_s\frac{H}{K}\cos(\theta - \theta_0) \qquad (5)$$

In equation (5) saturation magnetization I_s and K_1 for 5% Ga sample were used and figure 26 is the plot of equation (5) varies as a function of θ.

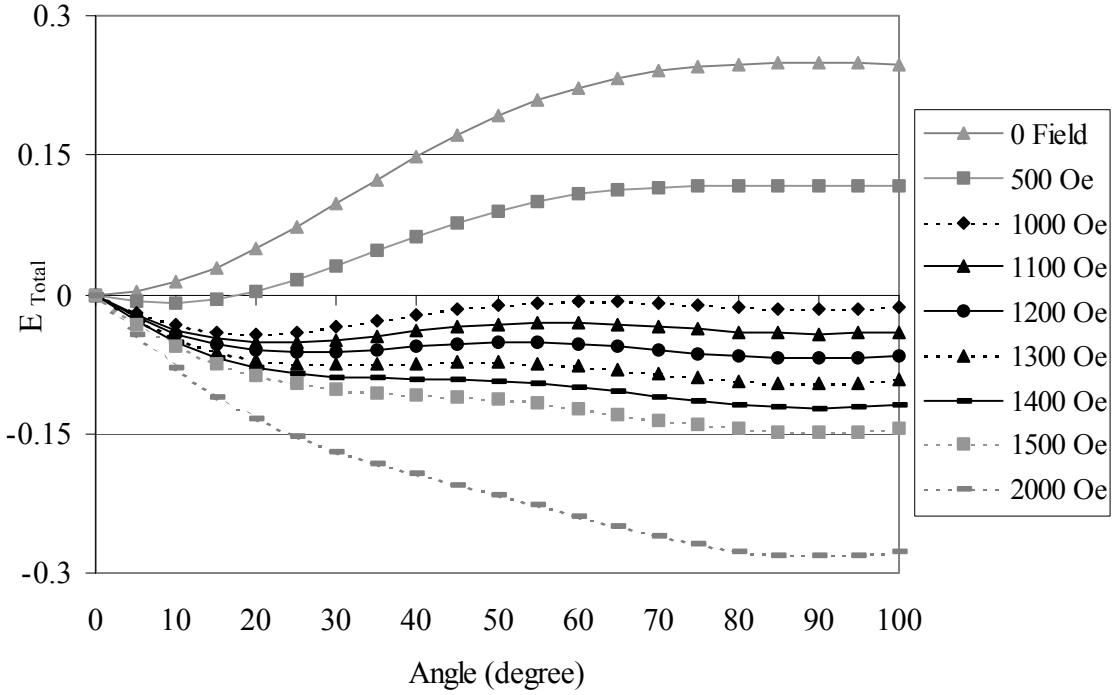

Figure 25: Total energy as a function of angle of magnetization with the easy axis when $K_2=-9K_1/4$.

From Figure 26 we can see that, without any external field applied field (when the total energy is equal to the anisotropy energy) there is not much difference in anisotropy energy in the material after we cross the direction <111>. This consistent with the magnetization curves shown in figure 23. With external field, as we can expect, the minima at $\theta = 0^o$ (the easy <100> axis direction) and the maxima along the hard direction at $\theta = 90^o$ (<110> direction) change. The minima at $\theta = 0^o$ shifts and the maxima at $\theta = 90^o$ gradually reduces. Ultimately with high enough field the minima at $\theta = 0^o$ vanishes and shifts to $\theta = 90^o$. But the energy curves in figure 25 clearly show that between 1000 Oe and 1300 Oe two minima exists, one at $\theta \approx 20^o$ and the other at $\theta = 90^o$. This suggests that we should see a

jump in magnetization around the applied field value of 1000 to 1300 Oe. But none of the experimental magnetization curves (Figure 13 to Figure 19) exhibits such jump or discontinuity in magnetization. As long as $|K_2|$ is smaller than $9K_1$ (which is valid for FeGa alloys according to the results obtained for this study) magnetization jump should exist when the applied field is along hard direction [16].

Figure 26 is the calculated magnetization curve.

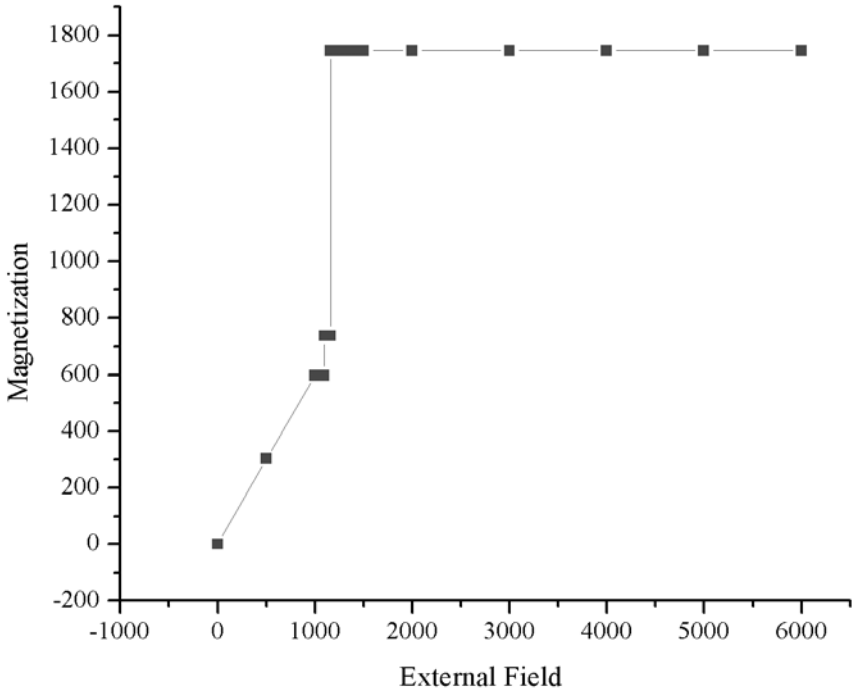

Figure 26: Calculated Magnetization Curve

For each applied field the position of the minimum (in terms of θ) was taken from Figure 25 and magnetization along field direction was calculated [$I_s \cos(90-\theta)$] and plotted against the corresponding field. As before I_s is the saturation magnetization for 5% Ga sample. We can see that the calculated magnetization

curve is very different from the experimentally obtained curves (Figure 13 to Figure 19).

One of the reasons for this discrepancy could be that the magnetization in the alloy is not homogeneous whereas homogeneous magnetization is an assumption of rotational model of magnetization. In references 12,13,18 and 19 there are indications that FeGa alloys have structural inhomogeneities. Also the fact that the relationship between the anisotropy constants holds true for $Ni_{51.3}Mn_{24.0}Ga_{24.7}$ for a range of temperature in the premartensitic phase can be best explained by saying that a premartensitic phase also exists in FeGa alloys. In that case the analysis of the anisotropy becomes different. So there are a number of possibilities that are beyond the scope of this report that could be contributing to the experimentally obtained interdependence of the anisotropy constants.

4. In order to have some idea about the magnetic domain patterns of FeGa alloys, MFM microscopy was used to image the magnetic layout. Figures 27–32 are the MFM images of different compositions.

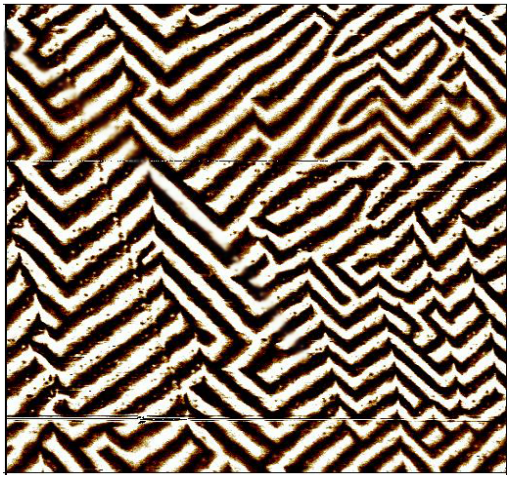

Figure 27: MFM image of
$Fe_{.95}Ga_{.05}$
Image area: 100 μm

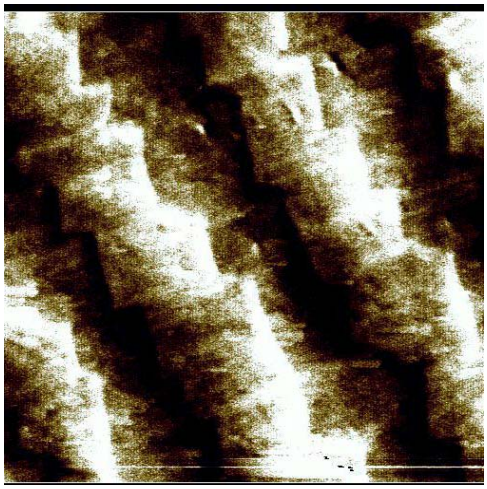

Figure 28: MFM image of
$Fe_{.95}Ga_{.05}$
Image area: 12 μm

Figure 29: MFM image of
$Fe_{.875}Ga_{.125}$
Image area: 10 μm

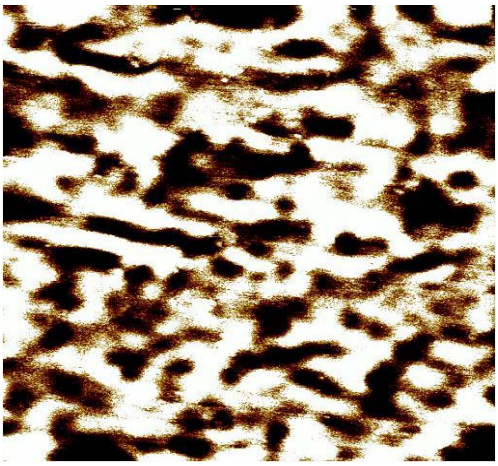

Figure 30: MFM image of
$Fe_{.875}Ga_{.125}$
Image area: 5 μm

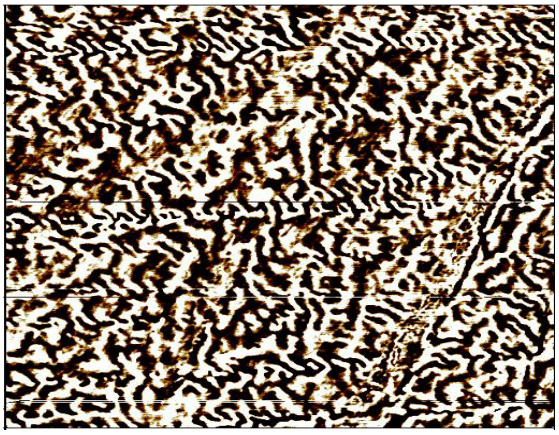

Figure 31: MFM image of $Fe_{.80}Ga_{.20}$
Image area: 50 μm

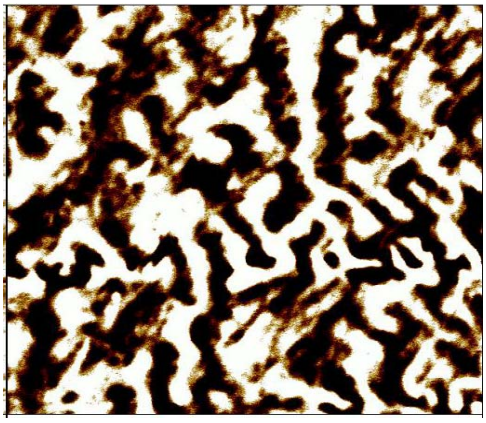

Figure 32: MFM image of $Fe_{.80}Ga_{.20}$
Image area: 15 μm

Though the details of these figures were not investigated but the difference in the magnetic images among different compositions is evident from observation. Magnetic domain image of a 5 % Ga sample seems to have an ordered pattern and is close to magnetic domain pattern of Fe [14]. But for 20% Ga the domain image is completely different which is an indication that magnetic properties change to a great extent with composition for FeGa alloys.

5.2 Future work

Following features, if investigated in future, will be able to establish more explicit nature of this alloy system:

- The second anisotropy constant K_2 for FeAl or FeGaAl alloys can be investigated. That will be able to explain if magnetic equivalence of two hard directions

(<110> and <111>) is unique to FeGa alloy or is an inherent property of these substitution iron alloys.

- Measurement of K_1 and K_2 by some other method (for example by torque magnetometry) to independently verify the trend of the constants with the composition and also the special relationship between them.
- The similarity of relationship of K_1 and K_2 between quenched FeGa alloys and NiMnGa can be further investigated.
- Measuring the anisotropy constants for $Fe_{1-x}Ga_x$ alloys with $x>0.2$ will be interesting to see if the constants continue to be small or there is any similarity with those of FeAl alloys.
- The magnetic domain images can be investigated further. The structure and properties of the domains might help to explain the magnetic anisotropic properties of the alloy for different compositions.

Appendix

I. Operating principle of VSM:

A VSM operates on Faraday's Law of Induction, that a changing magnetic field will produce an electric field. This electric field can be measured and can give information about the changing magnetic field. Figure 13 shows the schematics of a typical VSM magnetometer.

When a magnetic sample is placed in a constant magnetic field, the field will magnetize the sample by aligning the magnetic domains, or the individual magnetic spins, with the field. The magnetic dipole moment of the sample will create a magnetic

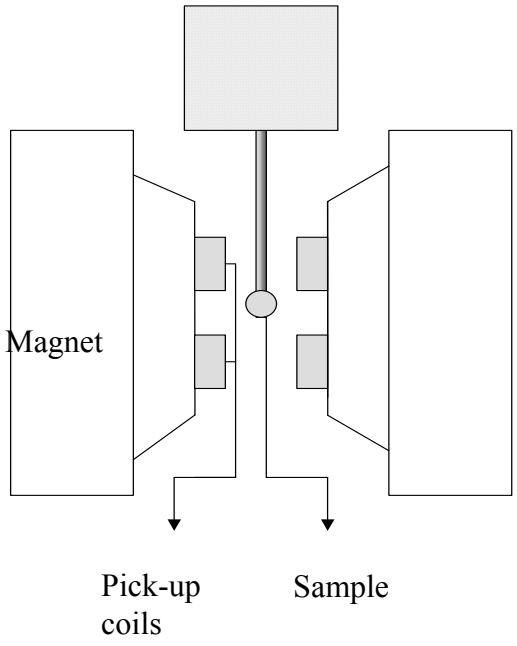

Figure 33: Schematic diagram of a VSM magnetometer.

field around the sample, sometimes called the magnetic stray field. As the sample is mechanically vibrated, this magnetic stray field changes as a function of time and this alternating magnetic field will cause an electric field in the pick-up coils. This current will be proportional to the magnetization of the sample. The greater the magnetization, the greater the induced current. A transimpedance amplifier and lock-in amplifier amplify the induction current. The various components are hooked up to a computer interface and the monitoring software gives information about the magnetization of the sample. A typical measurement of a sample is taken in the following manner:

- The strength of the constant magnetic field is set.
- The sample begins to vibrate
- The signal received from the probe is translated into a value for the magnetic moment of the sample
- The strength of the constant magnetic field changes to a new value. No data is taken during this transition
- The strength of the constant magnetic field reaches its new value
- The signal from the probe again gets translated into a value for the magnetization of the sample
- The constant magnetic field varies over a given range, and a plot of magnetization (M) versus magnetic field strength (H) is generated.

Different Parts of the VSM

The VSM consists of ten parts:

- water cooled electromagnet and power supply
- vibration exciter and sample holder (with angle indicator)
- sensor coils
- Hall probe
- amplifier
- control chassis
- lock in amplifier
- meter
- computer interface

Water cooled electromagnet and power supply

The water cooled electromagnet, along with the power supply, generate the constant magnetic field used to magnetize the sample.

Vibration exciter and sample holder (with angle indicator)

The sample holder rod is attached to the vibration exciter, and the end of it hangs down in between the pole pieces. The exciter moves the sample up and down at a set frequency, typically 85Hz. The sample rod can be rotated to achieve the desired orientation of the sample to the constant magnetic field. There are also three knobs for controlling the x,y, and z positions of the sample.

Sensor coils

The sample produces an alternating current in these coils at the same frequency as the vibration of the sample. The signal generated contains the information about the magnetization of the sample.

Amplifier

The amplifier amplifies the signal created by the sensor coils.

Control chassis

This controls the 85Hz oscillation of the exciter.

Lock in amplifier

This amplifier is tuned to pick up only signals at the vibrating frequency. This eliminates noise from the environment, such as from the overhead lights or hovering spacecraft nearby (unless the noise happens to be an 85Hz signal).

Computer Interface

The software makes data collection easier by automating the control of the various components during data collection. The data can be graphed and plotted on the printer.

One of the disadvantages of VSM is that the signal in the coils is very small (the signal caused by the before mentioned 10 nAm^2 is only a few nano-Volts) and therefore

extremely sensitive to noise sources. One of the major causes of problems in such a system is vibration of the coils relative to the field applied by the electro-magnet. The flux produced by the magnetic sample is approximately 1.0E-15 times smaller than the flux produced by the magnet; therefore vibrations must be canceled out by the same factor. The other problem of the particular VSM used for this study was that it could achieve maximum field value of 7 kOe though the design maximum field value is 10 kOe. But as far as the samples used for this study were concerned 7 kOe was enough to attain saturation.

References

1. R.C. Hall, Journal of Applied Physics, 1959. **30**(6): p. 816.
2. E. Tatsumoto and T. Okamoto, Journal of Physical Society of Japan, 1959. **14**: p. 1588.
3. R. C. Hall, Journal of Applied Physics, 1960. **31**(6): p. 1037.
4. T. B. Massalski, ed. *Binary Alloy Phase Diagram*. 2nd Edition, ASM International. 1990: Materials Park, Ohio, p.1064.
5. Nobuo Kawamiya, Kengo Adachi and Yoji Nakamura, Journal of Physical Society of Japan, 1972. **33**(5): p. 1318.
6. H. Leamy, E.D. Gibson, and F.X. Kayser, Acta Metallurgica, 1967. **15**: p. 1827.
7. A.E. Clark, James B. Restorff, Marilyn Wun-Fogle, Thomas A. Lograsso and Deborah L. Schlagel, IEEE Transaction on Magnetics, 2000. **36**(5): p. 3238.
8. J.R. Cullen, A.E. Clark, M. Wun-Fogle, J.B. Restorff, T. A. Lograsso, Journal of Magnetism and Magnetic Materials, 2001. **226-230**: p. 948.
9. Arthur E. Clark, Marilyn Wun-Fogle, James B. Restorff, Thomas A. Lograsso and James R. Cullen, IEEE Transaction on Magnetics, 2001. **37**(4): p. 2678.
10. A.E. Clark, K. B. Hathaway, M. Wun-Fogle, J.B. Restorff, T. A. Lograsso, V. M. Keppens, G. Petculescu, R. A. Taylor, Journal of Applied Physics, 2003. **93**(10): p. 8621.
11. M. Wuttig, L. Dai, and J.R. Cullen, Applied Physics Letters, 2002. **80**(7): p. 1135.
12. T.A. Lograsso, A.R. Ross, D.L. Schlagel, A.E. Clark, M. Wun-Fogle, Journal of Alloys and Compounds, 2003. **350**(95).
13. R. Wu, Journal of Applied Physics, 2002. **91**(10): p. 7358.

14. R.M. Bozorth, *Ferromagnetism*. 1951, New York: D. Van Nostrand Company Inc., p. 534, 592.

15. E.P Wohlfrath, ed. *Ferromagnetic Materials I*. Vol. 1. 1980, North Holland Publishing Co.: New York. p. 20,39.

16. A. Huber and R. Schafer, *Magnetic Domains: The Analysis of Magnetic Microstructures*. 1998, New York: Springer-Verlag Berlin Heidelberg New York, p. 192-195.

17. R. Tickle and R.D. James, Journal of Magnetism and Magnetic Materials, 1999. **195**: p. 627.

18. N. Koda, *TEM Analysis of FeGa Alloys*, MS Thesis, *Materials Science and Engineering*. 2003, University of Maryland: College Park.

19. D. Vieland, J.F. Li, T.A. Lograsso, A. Ross, Manfred Wuttig, Applied Physics Letters, 2002. **81**(17): p. 3185.